https://doi.org/10.5194/egusphere-2026-3634
Preprint. Discussion started: 8 July 2026

Machine Learning-Based Observational Constraints on Cloud Condensation Nuclei Responses to Australian Wildfire Aerosols over Remote Oceans

Boxin Yu[1], Jaswant Moher[1], Nadine Unger[1], James A. King[1], Ying Chen[1]*

[1]School of Geography, Earth and Environmental Sciences, University of Birmingham, Edgbaston, B15 2TT, Birmingham, UK

Correspondence to: Ying Chen (y.chen.21@bham.ac.uk)

Abstract. Australian "Black Summer" wildfires in 2019-2020 released large amounts of smoke that affected aerosols and clouds over the South Pacific. Here we quantified wildfire perturbation on aerosol loading and cloud condensation nuclei (CCN, particles that can act as seeds for cloud droplets) using a machine learning (ML) method. We trained ML models with meteorological datasets to represent counterfactual "no-wildfire" conditions, which were contrasted against satellite observations of "wildfire" conditions of aerosol optical depth (AOD), Aerosol Index, and CCN. We found strong and robust aerosol and CCN responses during the wildfire months over the South Pacific downwind plume region (140° E–100° W, 10° S–50° S). The wildfire perturbation substantially increased AOD by 36 % and 68 % in December 2019 and January 2020, respectively, and Aerosol Index by 21 % and 53 %, respectively. In comparison, CCN increased by 40 % in December 2019 and 20 % in January 2020. We find that the AOD and Aerosol Index enhancements form a broad band following the main smoke plume and extend across the full studied region over the South Pacific, while the CCN response is weaker and more localized, with enhancements mainly confined to the plume central-line along the main smoke transport pathway with a rapid decay further downwind. This difference suggests that transport and aging processes could reduce wildfire aerosol capability in enhancing CCN number concentration. Moreover, our results provide further observational evidence that Aerosol Index can provide a useful complement to AOD when interpreting smoke impacts on CCN.

1 Introduction

In recent years, wildfire frequency and intensity have increased worldwide, becoming a major source of atmospheric aerosol loading, and are expected to keep increasing in a warmer future (Huang et al., 2023; Zheng et al., 2020). Beyond degrading air quality, wildfire smoke can perturb cloud microphysics, atmospheric radiation, and regional to global climate through both aerosol–radiation and aerosol-cloud interactions (Sokolik et al., 2019). As highlighted in the Sixth Assessment Report (AR6) of the Intergovernmental Panel on Climate Change (IPCC), these effects are especially important because cloud-mediated radiative forcing remains a major source of uncertainty in climate assessment. In particular, marine low clouds are a strong cooling influence on the planet while remaining a leading source of uncertainty in climate sensitivity (Calvin et al.,

https://doi.org/10.5194/egusphere-2026-3634
Preprint. Discussion started: 8 July 2026

2023; Myers et al., 2021; Scott et al., 2020). One key reason for this uncertainty is that wildfire aerosols can act as cloud condensation nuclei (CCN, particles that can act as seeds for cloud droplets), increasing cloud droplet number concentration and decreasing droplet effective radius, thereby enhancing cloud albedo through the Twomey effect and producing a cooling tendency (Twomey, 1977). Previous observational and modelling studies have shown that aerosol perturbations, including biomass burning aerosols, can modify cloud droplet number concentration (CDNC), cloud albedo, and cloud cover, thereby influencing cloud-mediated radiative effects (Chen et al., 2015; Chen and Wang, 2016; Herbert and Stier, 2023; Kaufman and Koren, 2006; Liu et al., 2020; Roberts et al., 2003). However, the magnitude and climatic relevance of wildfire-induced cloud radiative forcing remain insufficiently constrained (Gryspeerdt et al., 2023). Because aerosol-cloud interactions are mediated through changes in CCN (Köhler, 1936; Twomey, 1974). It represents one of the largest sources of uncertainty in current climate projections (Forster, P. et al., 2023). However, direct CCN measurements remain sparse and sample only a small fraction of the globe, providing insufficient constraints on the global distribution of aerosols (Andreae, 2009; Spracklen et al., 2011; Stier, 2016). Research on CCN impacts over remote oceans is especially limited due to the sparse availability of CCN observations. Against this broader climatic background, the 2019–2020 'Black Summer' wildfires in Australia (hereafter 'AU wildfire(s)') provide an exceptional large-scale smoke perturbation for investigating wildfire impacts in a remote marine environment. It represents one of the most severe biomass burning events on record in the Southern Hemisphere (Ma et al., 2024; Peterson et al., 2021). The event released approximately 715 million tons of CO^2 -equivalent greenhouse gases (van der Velde et al., 2021). The event generated an unprecedented smoke plume rich in absorbing black carbon and scattering organic carbon. This plume was injected into the upper troposphere and even the stratosphere, causing significant warming in the Southern Hemisphere's lower stratosphere for over six months (Damany-Pearce et al., 2022; Li et al., 2026; Yu et al., 2021). Satellite observations from the Moderate Resolution Imaging Spectroradiometer aboard NASA's Aqua platform (Aqua-MODIS) recorded a clear temporal evolution of the smoke loading: aerosol optical depth (AOD) remained near background levels (0.026) in June 2019, rose sharply to a peak of 0.068 in December 2019, and gradually returned to background levels (0.027) by May 2020 (Yang et al., 2021). Observations from the Cloud-Aerosol Lidar with Orthogonal Polarization (CALIOP) instrument aboard the Cloud-Aerosol Lidar and Infrared Pathfinder Satellite Observation (CALIPSO) satellite further showed that the smoke was primarily distributed within the 0.5–4 km altitude range, with peak concentrations between 0.5 and 2 km (Ohneiser et al., 2020; Yang et al., 2021). Driven by the prevailing westerlies, this plume was transported across the South Pacific Ocean and reached South America within approximately 8–14 days (Ohneiser et al., 2020). This AU wildfire smoke was transported almost immediately over the remote South Pacific, largely unaffected by confounding continental pollution sources. This combination of exceptional emission scale, detailed spatiotemporal evolution, and a uniquely clean oceanic transport pathway make this AU wildfire an ideal 'natural experiment' for investigating wildfire impacts on aerosols and CCN over remote marine regions.

AOD, defined as the vertically integrated extinction of solar radiation by aerosol particles (Ångström, 1929), has therefore been widely adopted as a satellite-observable proxy for CCN concentration (Ahn et al., 2021; Block et al., 2024; Rosenfeld et al., 2008, 2023). However, AOD does not provide explicit information on the vertical distribution of aerosols; therefore,

https://doi.org/10.5194/egusphere-2026-3634
Preprint. Discussion started: 8 July 2026

aerosol layers above cloud base can increase AOD, but may not contribute to the CCN population relevant to low-level cloud formation (Painemal et al., 2020; Stier, 2016). In situ aircraft observations also demonstrate that aerosol optical properties can vary strongly with altitude, so surface or column-integrated measurements alone may not sufficiently constrain aerosol radiative impacts (Tian et al., 2020). In addition, AOD is influenced not only by particle number concentration but also by hygroscopic growth. Hygroscopic growth increases particle size and enhances optical extinction, but particle number concentration remains unchanged (Jin et al., 2023; Liu and Li, 2014). The relationship between CCN and AOD varies significantly between marine and continental regions, as well as across different aerosol environments (Stier, 2016). AOD can be an unreliable proxy for CCN in clean marine regions, where background AOD is dominated by coarse-mode sea salt aerosol, such that fine-mode CCN perturbations produce only a small AOD signal that is difficult to distinguish from natural background variability (Painemal et al., 2020). Consequently, over approximately 71 % of the global ocean area, the correlation between CCN and AOD falls below 0.5 (Stier, 2016). The Ozone Monitoring Instrument (OMI) Aerosol Index is derived from the departure of measured near-UV reflectance from that of a pure Rayleigh atmosphere (Torres et al., 1998). Other studies have suggested that Aerosol Index could act as a superior proxy for CCN, because it gives lower weight to large particles. Aerosol Index effectively reduces the interference from sea salt and dust particles, leading to more sensitive to aerosol size information (Hasekamp et al., 2019; Ma et al., 2018; Stier, 2016). Studies have suggested that Aerosol Index is often more closely related to CCN than AOD across different aerosol environments (Hasekamp et al., 2019; Ma et al., 2018; Rosenfeld et al., 2023). Moreover, the OMI Aerosol Index is sensitive to absorbing aerosols, such as black carbon in smoke, and their vertical height (Jethva et al., 2018). Although Aerosol Index may better capture smoke-related and size-related aerosol information, both AOD and Aerosol Index remain column-integrated indirect proxies and cannot directly represent CCN concentration. Their relationship to CCN is mediated by composition, hygroscopicity, size distribution, supersaturation conditions, and vertical structure, factors that cannot be independently resolved from a single optical column quantity (Deng et al., 2011; Dusek et al., 2006a; Liu and Li, 2014; Petters and Kreidenweis, 2007; Stier, 2016). Therefore, jointly analyzing AOD, Aerosol Index, and CCN are important for constraining wildfire-induced aerosol perturbations.

Nevertheless, observation-based analysis of wildfire aerosol anomalies faces a key challenge: the observed variations in AOD, Aerosol Index, and CCN reflect not only emission enhancement but are also significantly influenced by meteorological conditions, such as boundary layer structure, hygroscopic growth, and large-scale transport (Chen et al., 2022, 2024). Consequently, only relying on observed anomalies makes it difficult to distinguish the relative contributions of meteorological variables and wildfire aerosols to changes in AOD, Aerosol Index and CCN. This limits the accurate quantification of wildfire-induced aerosol perturbations. Therefore, isolating the wildfire-driven CCN signal requires a method that can construct a reliable “no-wildfire” aerosol baseline under the same meteorological conditions as those actually occurring during the event.

Here, we address these challenges by developing a machine-learning counterfactual framework based on long-term observations of aerosol and CCN to isolate wildfire-induced perturbations in AOD, Aerosol Index, and column-integrated CCN from meteorological co-variability over the South Pacific during the 2019–2020 AU wildfire. We utilize ERA5

https://doi.org/10.5194/egusphere-2026-3634
Preprint. Discussion started: 8 July 2026

(Hersbach et al., 2020), the fifth-generation atmospheric reanalysis produced by the European Centre for Medium-Range Weather Forecasts (ECMWF) meteorological reanalysis data with satellite observations to train machine-learning models that estimate the "no-wildfire" baseline (Chen et al., 2022, 2024). This model constructs a meteorologically driven aerosol baseline, representing the expected states of AOD, Aerosol Index, and CCN under identical meteorological "no-wildfire" conditions. By comparing satellite observations of AOD, Aerosol Index, and CCN during the wildfire peak months (December 2019 and January 2020) against their meteorologically conditioned "no-wildfire" baselines, we isolate perturbations driven specifically by the wildfire smoke plume rather than by meteorological co-variability. The AU wildfire case provides a valuable opportunity to understand the smoke plume's impact on AOD, Aerosol Index and CCN, and to evaluate the fidelity of AOD and Aerosol Index as proxies of CCN for smoke aerosol over south Pacific marine conditions.

2 Materials and methods

2.1 Satellite observations of aerosol and CCN

We used Level-3 monthly AOD and cloud products of Moderate Resolution Imaging Spectroradiometer (MODIS) satellite collection 6.1 during 2003-2024. The MODIS collection 6.1 corrects the instrumental degradation and cloud optical property biases that were previously present in Terra-Collection 5.1, so that now both Terra-MODIS and Aqua-MODIS show consistent results.

We used the Level-3 daily global gridded OMI/Aura UV Aerosol Index product from the TOMS-like dataset (OMTO3d, Version 3) for 2005–2024 (Pawan K. Bhartia, 2012). In our processing, we aggregated the daily data into monthly means for use in the analysis to be consistent with MODIS dataset.

A global CCN dataset during 2007-2021, the available period of the CALIPSO-derived CCN product, was also used in this study (Choudhury and Tesche, 2023). It provides a multiyear height-resolved dataset of aerosol-type specific CCN concentrations estimated from the space-borne lidar aboard the CALIPSO satellite launched in April 2006. To ensure spatial consistency with the 1°×1° ERA5 grids, the original monthly data of CCN from all aerosol types was regridded to 1°×1° from original 2°×5° data using bilinear interpolation by independently applying it to each time-altitude slice on a global regular latitude-longitude grid. To be consistent with AOD and Aerosol Index, both of which represent aerosol column properties, we constructed a column-integrated CCN dataset for 1000–200 hPa to represent the total CCN in the troposphere. The three satellite datasets span different periods due to the operational timelines of their respective missions. These differing periods do not affect our analysis, as each variable's machine-learning model is trained independently using its own full available dataset.

2.2 ERA5 Meteorological reanalysis

The meteorological parameters from ERA5 were collocated with Terra-MODIS and Aqua-MODIS overpass time during daytime (Hersbach et al., 2020). Meteorological variables from ERA5 were aggregated spatially to 1°×1° resolution and

https://doi.org/10.5194/egusphere-2026-3634
Preprint. Discussion started: 8 July 2026

temporally to monthly means to match the AOD and Aerosol Index datasets. For analysis of AOD, Aerosol Index and CCN, the machine learning (ML) used meteorological variables from surface to 200 hPa. The original names of the surface and pressure level variables from ERA5 are given in Table A1.

2.3 Machine learning

Observational relationships between aerosol and CCN (or cloud properties) can be strongly confounded by meteorological co-variability, which complicates the interpretation of aerosol-driven effects (Chen et al., 2022, 2024; Christensen et al., 2022). To disentangle wildfire-induced signals from these confounding factors, we developed a ML model to estimate target variables (AOD, Aerosol Index, or CCN) based on given meteorological conditions. All observational data from the AU wildfire period (December 2019 to May 2020) and historical wildfires months before 2020 were strictly excluded from the training dataset, allowing ML to learn the counterfactual "no-wildfire" conditions. The wildfire perturbation was quantified by comparing satellite observations during the wildfire months against the ML estimated "no-wildfire" conditions. This study used the Random Forest regression algorithm. Random Forest is a widely used ensemble-learning algorithm that performs well in estimating nonlinear relationships in high-dimensional feature spaces, is relatively robust to overfitting, and provides feature importance for model interpretation (Belgiu and Drăguţ, 2016; Breiman, 2001; Scornet et al., 2015). There have been many studies showing the use of Random Forest algorithms to successfully predict PM2.5 using parameters including meteorological variables (Bi et al., 2022; Brokamp et al., 2018; Lv et al., 2021). Using ERA5 meteorological variables as inputs, we trained three independent Random Forest models, one for each target variable: MODIS AOD, OMI Aerosol Index, and CALIPSO column-integrated CCN. The trained ML models act as a surrogate of the satellite datasets to represent the counterfactual observations in "no-wildfire" conditions, and are referred to as ML-MODIS, ML-OMI, and ML-CALIPSO, respectively.

The satellite observations during the target period, influenced by wildfire emissions, were compared with the ML estimates for this period under identical meteorological conditions. Thus, this approach allows isolation and quantification of the specific contributions from wildfire. To focus the ML more on regional-specific relationships between local meteorology and aerosol/CCN variability, we adopt a stratified training strategy by dividing the study area (140° E–100° W, 10° S–50° S) into twelve 20°×20° subdomains and train 12 ML models separately for AOD, Aerosol Index and CCN (Li et al., 2019; Xiao et al., 2018). Only oceanic regions were analyzed to focus on marine clouds that have larger impacts on radiative forcing than clouds over continents.

To estimate the uncertainty of the ML-MODIS, ML-OMI, and ML-CALIPSO estimates, we used a leave-two-years-out cross-validation (LTYO) Monte Carlo ensemble approach (Chen et al., 2024). For each ensemble member, we randomly excluded two years of data (with replacement) and trained ML using the remaining years. This procedure was repeated to generate an ensemble of 1000 members, allowing us to estimate the uncertainty of the machine-learning estimate.

https://doi.org/10.5194/egusphere-2026-3634
Preprint. Discussion started: 8 July 2026

3 Results and discussion

3.1 Responses of AOD and Aerosol Index to the Australian wildfire

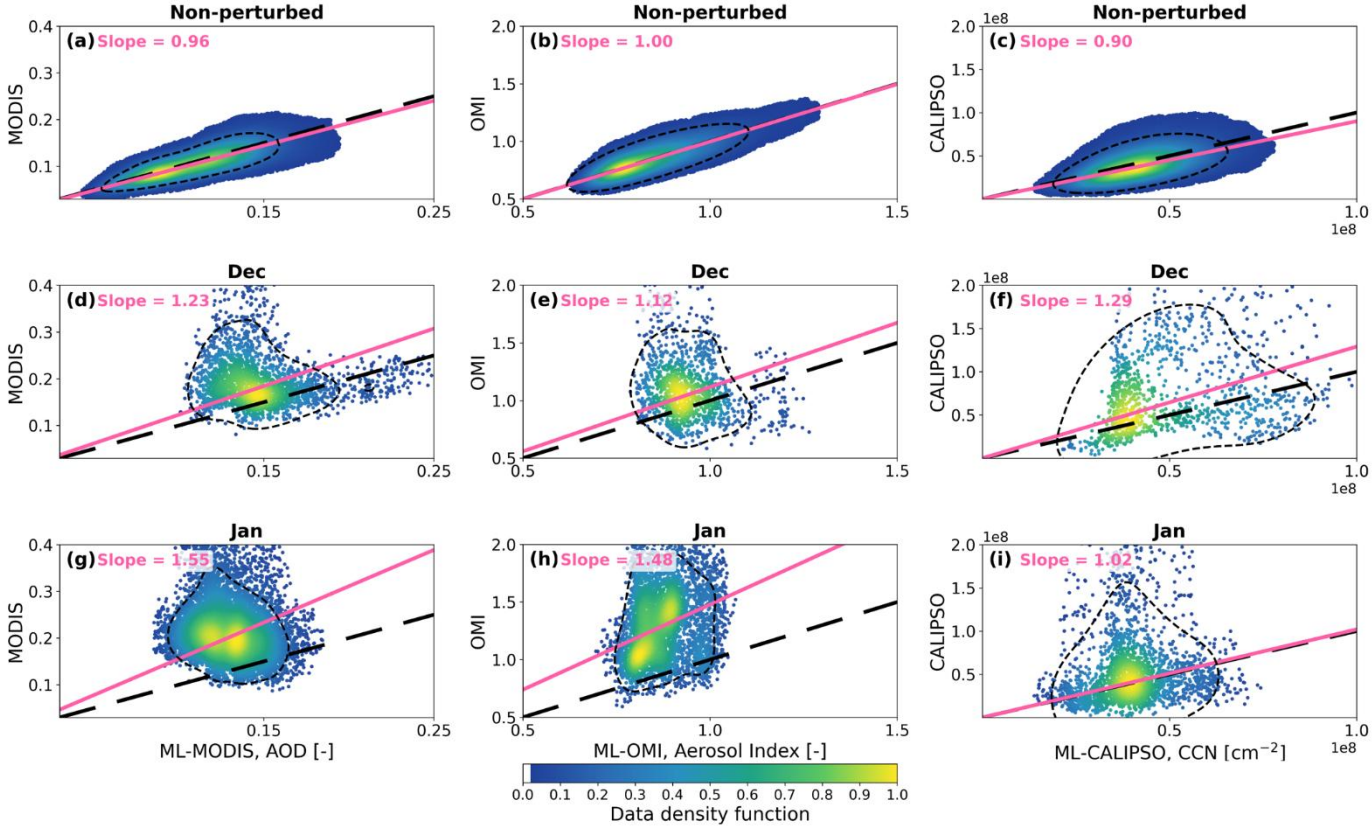

Figure 1: Scatter density plots of satellite observations versus ML estimates for AOD, Aerosol Index, and CCN.

The top row (a, b, c) evaluates the non-perturbed baseline via leave-two-year-out cross-validation. The middle and bottom rows display the wildfire months (Dec 2019, Jan 2020). The color scale (dark blue to yellow) represents the normalized data density function, with yellow indicating the highest density of points. Pink lines are linear regressions (slopes indicated), thick black dashed lines are 1:1 references, and thin dashed contours outline the 80 % core data distribution of the non-perturbed baseline to highlight wildfire-induced positive anomalies.

To isolate wildfire-driven aerosol signals from meteorological signals, we applied the trained ML models as described in Sect. 2.3 to estimate the expected "no-wildfire" aerosol conditions during December 2019 and January 2020. Figure 1 illustrates the scatter plot relationship between satellite observations (MODIS, OMI, and CALIPSO) and ML-based estimates (ML-MODIS, ML-OMI, and ML-CALIPSO) for December 2019, January 2020, and the non-perturbed LTYO samples. Overall, the non-perturbed samples (Figs. 1a, 1b, and 1c) are primarily aligned along the 1:1 line, with slopes of

https://doi.org/10.5194/egusphere-2026-3634
Preprint. Discussion started: 8 July 2026

175 0.96, 1.00, and 0.90 for AOD, Aerosol Index, and CCN. The average Pearson r values for AOD and Aerosol Index across 12 subdomains are in the range of 0.84 and 0.90, respectively, indicating good fidelity. These correlations are statistically significant ($P < 0.001$). These non-perturbed plots demonstrate that the meteorological baseline effectively captures the background variability and interannual fluctuations of AOD, Aerosol Index and CCN within the study domain. Figures 1d, e, f, g, h, and i clearly show a deviation during the Australian wildfire months (December 2019 and January 2020). The
180 observed AOD and Aerosol Index are substantially higher than the ML estimated “no-wildfire” baseline, indicating strong AU wildfire influence.

https://doi.org/10.5194/egusphere-2026-3634
Preprint. Discussion started: 8 July 2026

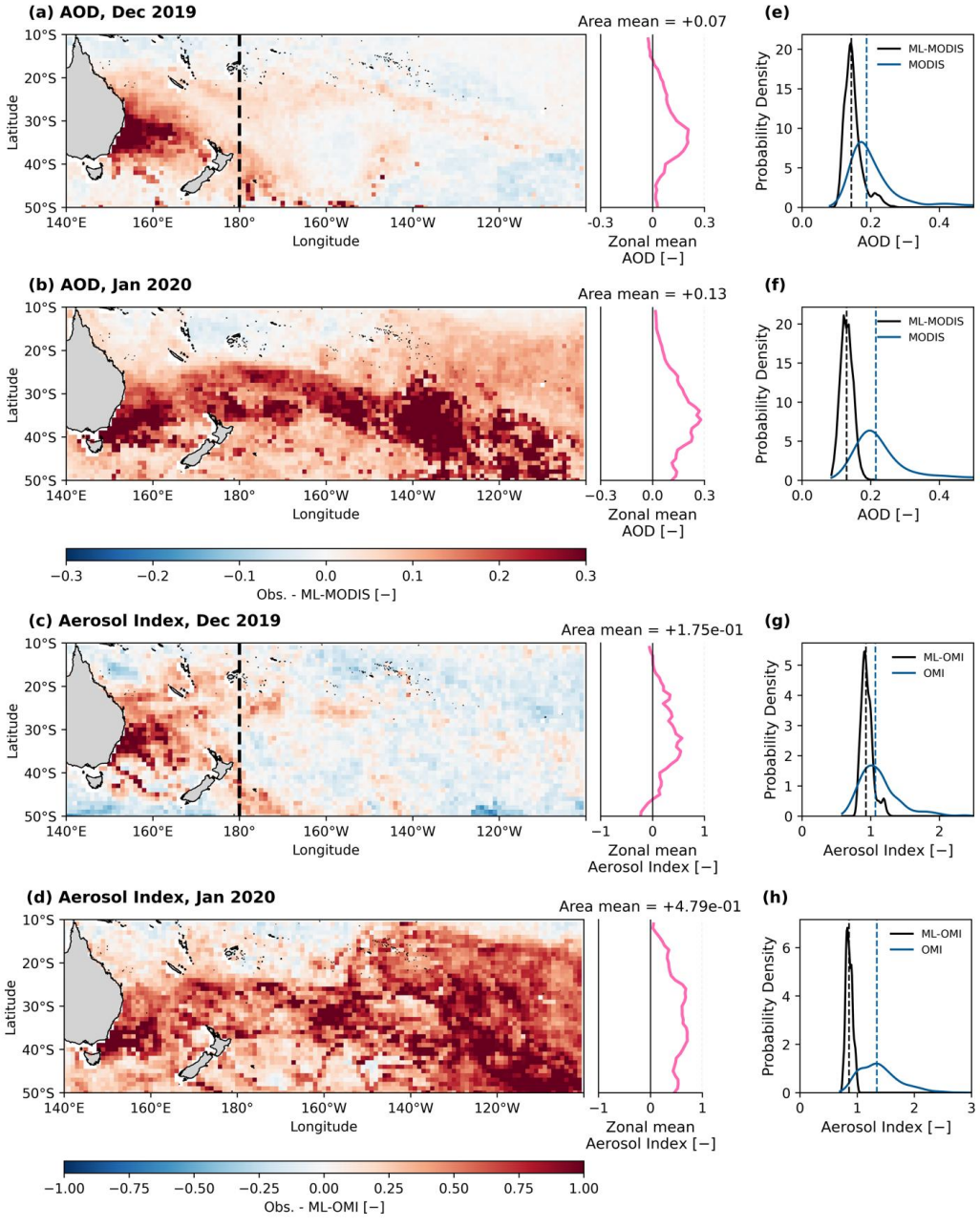

Figure 2: Spatial responses of AOD and Aerosol Index to wildfire perturbations estimated from the differences between MODIS/OMI observations and ML estimates (Obs. - ML).

(a, b) AOD perturbation maps for December 2019 and January 2020, respectively. (c, d) Aerosol Index perturbation maps for December 2019 and January 2020, respectively. The middle sub-panels show the corresponding zonal-mean perturbation profiles. In panels (a) and (c), the area to the left of the black dashed line is the research area used for zonal mean and

https://doi.org/10.5194/egusphere-2026-3634
Preprint. Discussion started: 8 July 2026

probability density analysis (140° E-180°, 10° S-50° S). Regional-mean statistics were calculated as area-weighted averages. In panels (e–h), the black and blue dashed lines represent the medians values of ML-MODIS/ML-OMI estimates and MODIS/OMI observations, respectively.

We compared the satellite observations from December 2019 and January 2020 with the corresponding non-perturbed conditions (Fig. 2). Both months show significant positive perturbations along the smoke transport path. The zonal-mean in Fig. 2 shows that perturbations in AOD and Aerosol Index indicate clear peaks across different longitudes. Overall, the peak values and the area of influence in January 2020 are stronger than in December 2019. The corresponding probability density results show that the perturbed distributions of AOD and Aerosol Index shift toward larger values compared to the "no-wildfire" background, with a much larger shift in January 2020.

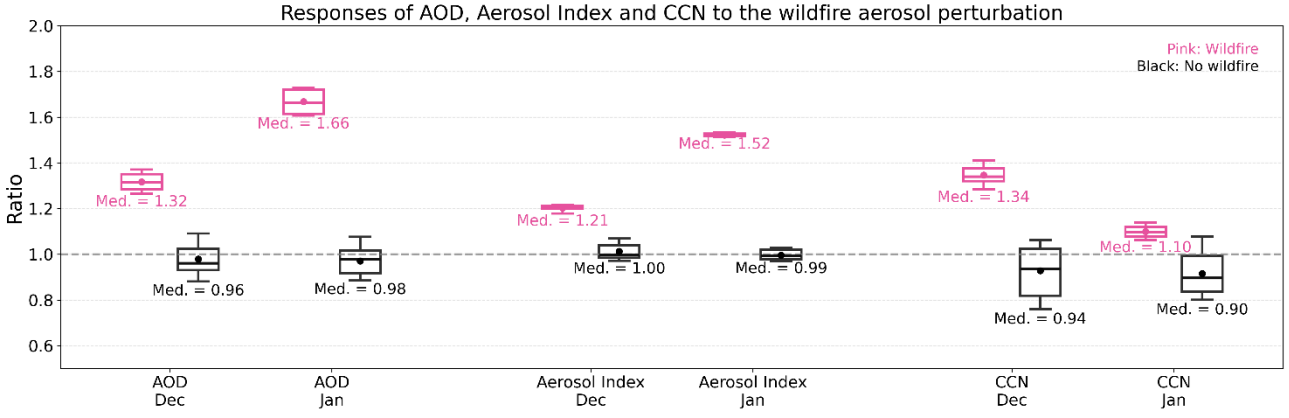

Figure 3: Responses of AOD, Aerosol Index and CCN to the wildfire aerosol perturbation in December 2019 and January 2020.

The y-axis represents the ratio of satellite observations to the ML estimate of "no-wildfire" cases under the same meteorological conditions. Pink boxes indicate the distributions during the wildfire perturbation, while black boxes represent the non-perturbed baseline derived from a Monte Carlo method. For each boxplot, the horizontal line inside the box indicates the median, and the dot represents the mean. The top and bottom edges of the box represent the 75th and 25th percentiles, respectively, and the whiskers extend to the 90th and 10th percentiles. The horizontal dashed gray line (Ratio = 1.0) indicates perfect agreement between satellite observations and ML surrogates.

Fig. 3 uses the ratio of satellite observations (MODIS, OMI, CALIPSO) to the corresponding surrogate satellites (ML-MODIS, ML-OMI, ML-CALIPSO) to represent the wildfire influences. To estimate uncertainty, we used the Monte Carlo ensemble as described in the Methods section. We estimated that in December 2019, the AU wildfire led to an increase in AOD, Aerosol Index, and CCN by 36 %, 21 %, and 40 %, respectively, on average across the whole studied region. In January 2020, the increases were much larger for AOD and Aerosol Index, 68 % and 53 %, respectively, and smaller for CCN at 20 %.

https://doi.org/10.5194/egusphere-2026-3634
Preprint. Discussion started: 8 July 2026

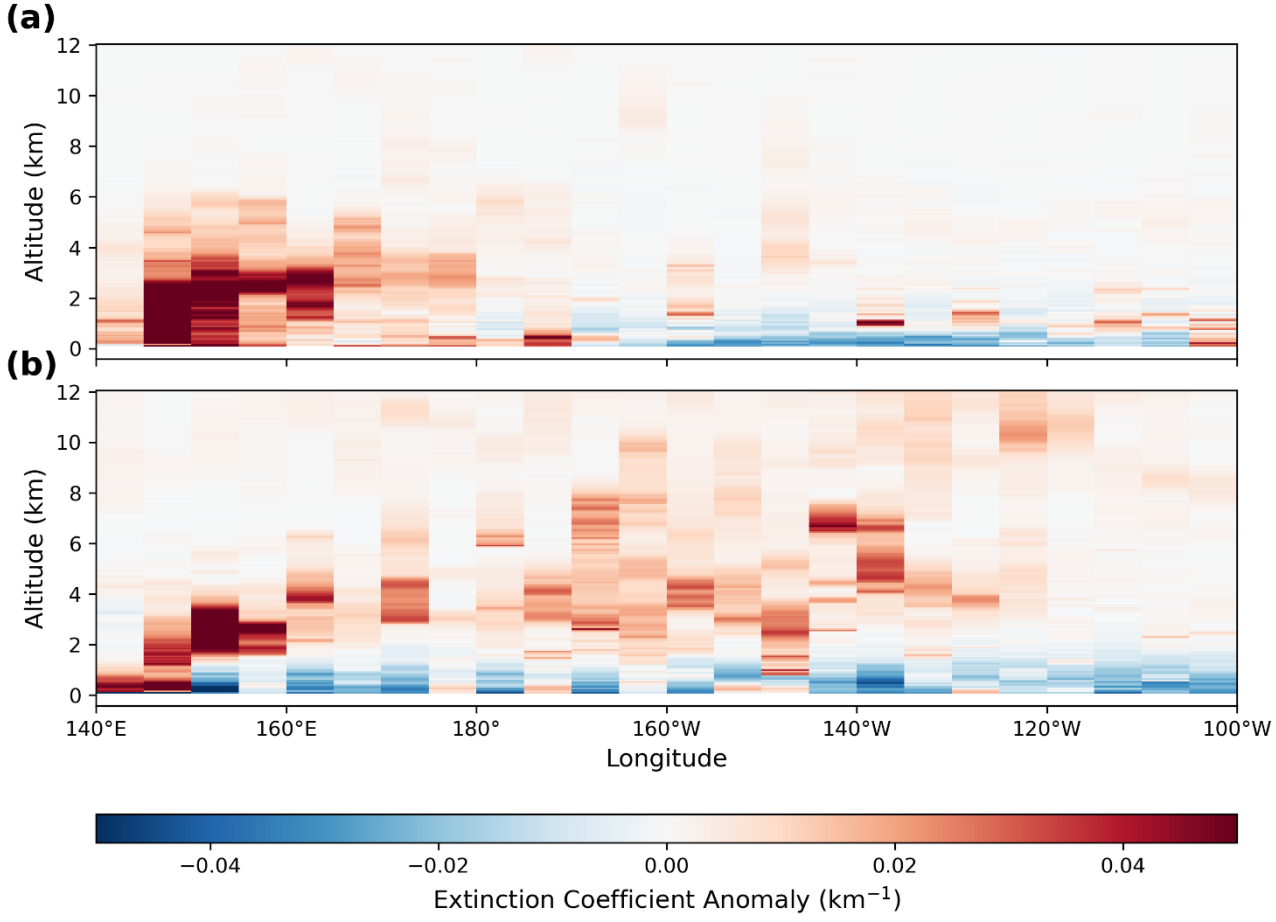

Figure 4: Vertical cross-sections of extinction coefficient anomalies along the 40° S–25° S latitudinal band for (a) December 2019 and (b) January 2020.

Anomalies are calculated relative to the 2007–2019 climatological mean for the corresponding months. The vertical axis denotes altitude (0–12 km) and the horizontal axis denotes longitude (140° E–100° W).

To identify which altitudes contribute most to AOD and to describe the vertical structure of the smoke plume, we analysed the climatological longitude–height profiles of the CALIPSO 532 nm extinction coefficient (Fig. 4). In December 2019, the extinction increase is mainly concentrated between 0 and 3 km near the wildfires. In January, as the wildfires intensified, the signal remained strong between 0.5 and 4 km, and the fire plume was transported further to west South Pacific. This vertical distribution, dominated by the lower layers, is consistent with previous CALIPSO observations (Ohneiser et al., 2020; Yang et al., 2021). The smoke signal reached 120° W, which was consistent with Fig. 2b. A large amount of smoke is lifted into the middle and upper troposphere and undergoes significant long-range transport across the Pacific Ocean, driven by the westerlies.

https://doi.org/10.5194/egusphere-2026-3634
Preprint. Discussion started: 8 July 2026

3.2 Localized Enhancements and Rapid Decay of Wildfire CCN

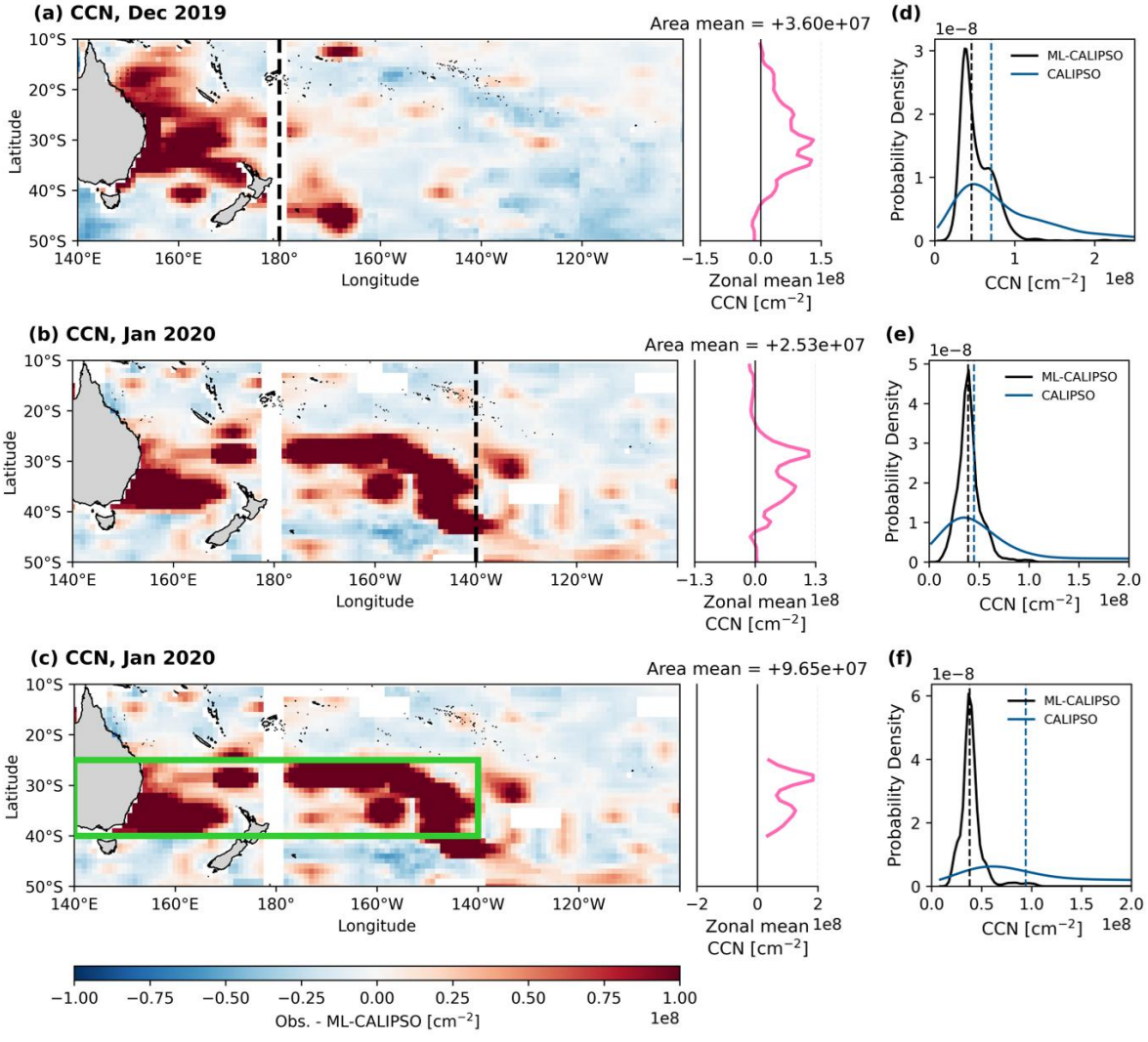

Figure 5: Spatial responses of CCN to wildfire perturbations are estimated from the differences between CALIPSO observations and ML-CALIPSO estimates (Obs. - ML).

Panels (a) and (b) show the CCN perturbations for December 2019 and January 2020, respectively. The area to the left of the black dashed line indicates the research area for zonal mean and probability density analysis, i.e., (140° E-180°, 10° S-50° S) for a) and (140° E-140° W, 10° S-50° S) for b). Regional-mean statistics were calculated as area-weighted averages. Panel (c) shows the January 2020 plume-core region highlighted by the green box, where the CCN enhancement is strongest and more spatially coherent. The dashed blue and black vertical lines in panels (d)–(f) indicate the median values of CALIPSO observations and ML-CALIPSO estimates, respectively.

https://doi.org/10.5194/egusphere-2026-3634
Preprint. Discussion started: 8 July 2026

We compared CALIPSO column-integrated CCN (1000–200 hPa) observations with a "no-wildfire" baseline (ML-CALIPSO) under the same meteorological conditions. When there was no wildfire in the real world, the ML-CALIPSO baseline reproduces the observed CCN variability reasonably well, with a mean Pearson r of ~0.89 across the 12 subdomains, and the correlations were statistically significant ($P < 0.001$), confirming that the ML model estimates a reliable "no-wildfire" baseline. Using this baseline, we quantified the CCN perturbations caused by wildfires (Fig. 5). Overall, positive CCN anomalies follow the smoke transport path, with the strongest signals around the plume central core (green box in Fig. 5c). Outside the plume central core, the response of CCN weakens rapidly. This is different from AOD and Aerosol Index, which have a much broader increase across the entire study area.

To study CCN perturbations more clearly, we selected an additional sub-region in the plume core (green domain) for further analysis in January (Figs. 5c and 5f). The zonal mean (pink line) shows that the peak of positive CCN perturbations is concentrated in the latitude band covered by the plume. However, when the entire study area is considered (Figs. 5d and 5e), the shift in the probability density median line is not obvious. This is because many grid points with weak or near-zero signals dilute the area-weighted average of CCN response. However, inside the green domain (Fig. 5f), the CALIPSO observed CCN distribution shows a clear rightward shift relative to ML-CALIPSO. This indicates that the CCN increase was mainly centered in the plume central core, rather than the large background area downwind. Quantitatively, according to Fig. 3, CCN increased by about 40 % in December 2019 but only by about 20 % in January 2020. This suggests that stronger aerosol loading did not always lead to proportional CCN enhancement, given the nonlinear relationship between AOD and CCN.

3.3 Relationship between AOD, Aerosol Index and CCN under wildfire conditions

In terms of spatial patterns and statistical distributions, wildfire plumes lead to a wider and more persistent increase in AOD/Aerosol Index. In contrast, the increase in CCN is more concentrated, and decays faster when the plume is transported further downwind following the westerlies or dispersed meridionally. Specifically, Fig. 2 shows that the positive AOD changes cover a larger downwind area. However, as shown in Fig. 5, the positive CCN anomalies are mainly limited to the plume central core and weaken quickly outside of it, with a regional average CCN increase of about 20 % in January, considerably lower than the corresponding increases in AOD (68 %) and Aerosol Index (53 %). Our ML approach detects significant enhancement in both AOD and CCN along the smoke transport pathway, suggesting that both are influenced by wildfire emissions. However, the responses of AOD and CCN are not proportional. Although higher AOD generally coincides with higher CCN, the CCN enhancement does not scale linearly with AOD, limiting the use of AOD alone as a direct proxy for CCN. This is consistent with previous studies (Liu and Li, 2014; Romakkaniemi et al., 2012).

AOD and CCN behave differently because they are sensitive to different aerosol features. AOD is mainly affected by aerosol mass loading and particle size (Jin et al., 2023). In contrast, CCN concentration is determined by both the absolute number of activatable particles and their hygroscopicity (κ) (Dusek et al., 2006; Edwards et al., 2021; Jin et al., 2023; Petters and Kreidenweis, 2007), hence CCN is more sensitive to the activatable aerosol number especially for the smaller size particles,

https://doi.org/10.5194/egusphere-2026-3634
Preprint. Discussion started: 8 July 2026

which usually have larger number concentration. Due to this difference, as the smoke plume moves and changes, AOD and CCN do not dilute at the same rate. Several processes during plume transport and aging could reduce CCN number but do not decrease AOD to the same extent. For example, first, intense coagulation near the source significantly reduces the particle number concentration and pushes particles into the accumulation mode which contributes largely to AOD (Hodshire et al., 2019; June et al., 2022; Ramnarine et al., 2019). Because coagulation conserves total aerosol mass and moves aerosol to more visible light sensitive accumulation mode but reduces aerosol number concentration by shifting particles toward larger sizes (Sakamoto et al., 2016), coagulation could increase AOD by reducing CCN. In addition, the accumulation mode particles have a relatively long atmospheric lifetime, favoring long-range transport (Chen et al., 2016). This keeps the total mass and extinction efficiency at high levels, making the AOD signal persist over further distances. However, the irreversible coagulation of particles leads to a rapid decay in the absolute number of effective CCN. This reduction in number and increase in size due to coagulation process is supported by high-resolution simulations and aircraft observations in biomass burning plumes (Hodshire et al., 2019; June et al., 2022; Ramnarine et al., 2019). Second, plume dilution and wet scavenging, especially in-cloud scavenging, first removes larger, activatable particles (Ding et al., 2019; Edwards et al., 2021; Pierce et al., 2007; Textor et al., 2006). These further speed up the loss of effective CCN number concentration downwind. In addition, chemical aging and mixing state evolution, such as secondary organic aerosol formation and mixing with soluble inorganic salts, during transport significantly increase the aerosol hygroscopicity (κ) and lower the activation supersaturation threshold (Sc) (Petters and Kreidenweis, 2007). As shown in previous studies, this microphysical aging can increase the CCN potential by several times within just a few hours (Reid et al., 2005; Vakkari et al., 2014). However, aging could also facilitate wet scavenging and hence speed up the decay of CCN response signal over the longer-term, although aging significantly improves the CCN activation in near source regions in short-term. Therefore, during long-range transport, even though downwind smoke particles are more hygroscopic, their low number concentration still causes the CCN signal to be more localized and decay faster than AOD.

Although the signal of AOD response is similar to the CCN response in the beginning phase of AU wildfire (Dec. 2019, Fig. 3), Aerosol Index response becomes closer to the CCN response than the AOD response in developed and aged phase in January 2020. Previous studies have noted that using AOD alone as a CCN proxy is not always stable (Liu and Li, 2014; Romakkaniemi et al., 2012). To better represent CCN, we need additional information about particle size features (Hasekamp et al., 2019; Liu and Li, 2014). Therefore, relying only on AOD to infer downwind CCN and potential aerosol-cloud interaction strength may lead to systematic biases. Aerosol Index is more sensitive to smaller particles (Jethva et al., 2018); therefore, Aerosol Index could be more relevant to CCN number concentration in some cases, e.g., Jan. 2020, and could be used as an additional proxy along with AOD to represent CCN in regions with sparse in-situ observations.

https://doi.org/10.5194/egusphere-2026-3634
Preprint. Discussion started: 8 July 2026

4 Conclusions

We used a satellite-based ML method to disentangle wildfire impacts on aerosol and CCN from meteorological noise. We quantified how the 2019–2020 Australian "Black Summer" wildfires disturbed aerosols and column-integrated CCN over the South Pacific. We validated the model and estimated the uncertainty with leave-two-year-out Monte Carlo ensembles. This framework can compare wildfire months with "no-wildfire" conditions under similar (identical) weather, which minimizes the effect of meteorological co-variability.

Over the full studied region (140° E–100° W, 10° S–50° S), the wildfires caused a strong and widespread aerosol signal. Compared with the ML "no-wildfire" counterfactual baseline, AOD increased by about 36 % in December 2019 and about 68 % in January 2020. Over the same months, the Aerosol Index increased by about 21 % and 53 %. Maps, zonal means, and probability density functions all show that the AOD and Aerosol Index increases over a very large region along the main smoke transport pathway, and the signal was stronger and wider in January 2020 than December 2019. Compared to aerosol responses over the wider South Pacific, the increase of CCN was mainly limited along the plume central line, and the enhanced signal decayed quickly in further downwind or dispersal regions.

These findings have important implications for understanding wildfire impacts on climate. CCN increases of 20-40 % could substantially perturb cloud microphysical properties and the associated radiative forcing (Chen et al., 2024; Jia et al., 2021; Quaas et al., 2020). Our results show that AOD (or Aerosol Index) and CCN do not scale linearly during wildfires. Transport, dilution, removal, and plume aging reduce CCN number more quickly than they reduce AOD/Aerosol Index. Therefore, AOD-based estimates of wildfire aerosol-cloud interactions may systematically misrepresent the spatial pattern of CCN perturbations and the resulting cloud radiative forcing, while Aerosol Index can provide a useful complementary proxy to AOD when interpreting smoke impacts on CCN. Future work should quantify the cloud microphysical and radiative forcing responses to the CCN perturbations. Due to future climate warming, the frequency and intensity of wildfires are expected to increase (Huang et al., 2023). Understanding these nonlinear aerosol-CCN-cloud relationships over remote oceans will be critical for constraining future wildfire-driven climate forcing.

Appendix A

We note that after regridding from 2° × 5° to 1° × 1°, the CALIPSO CCN fields show a narrow band of missing data near 180° longitude. This is caused by the combination of the original coarse grid and the longitude wrapping at the dateline during the regridding procedure, which leaves some 1° cells without valid source values. These grid cells were kept as missing values and excluded from subsequent spatial statistics.

https://doi.org/10.5194/egusphere-2026-3634
Preprint. Discussion started: 8 July 2026

Table A1. ERA5 monthly meteorological parameters

Surface Variables	Pressure Variables (1000 hPa to 200 hPa)
large_scale_rain_rate	divergence
100m_u_component_of_wind	geopotential
mean_sea_level_pressure	potential_vorticity
100m_v_component_of_wind	relative_humidity
precipitation_type	specific_humidity
10m_wind_speed	temperature
sea_ice_cover	u_component_of_wind
2m_dewpoint_temperature	v_component_of_wind
sea_surface_temperature	vertical_velocity
boundary_layer_height	vorticity
skin_temperature	
convective_available_potential_energy	
total_column_water_vapour	
friction_velocity	
total_precipitation	
instantaneous_10m_wind_gust	
instantaneous_moisture_flux	
k_index	
large_scale_precipitation_fraction	

330

Code and data availability

The MODIS cloud and aerosol products from Aqua (MYD08_L3) and Terra (MOD08_L3) used in this study are available from NASA Atmosphere Archive and Distribution System Distributed Active Archive Center (LAADS DAAC; https://ladsweb.modaps.eosdis.nasa.gov). The OMI/Aura Level-3 TOMS-like UV Aerosol Index product (OMTO3d, Version 3) is available from the NASA Goddard Earth Sciences Data and Information Services Center (GES DISC; https://disc.gsfc.nasa.gov). The CALIPSO-derived global multiyear three-dimensional cloud condensation nuclei dataset used in this study is available from PANGAEA at https://doi.org/10.1594/PANGAEA.956215. The CALIPSO aerosol

335

https://doi.org/10.5194/egusphere-2026-3634
Preprint. Discussion started: 8 July 2026

extinction data used for the vertical aerosol structure analysis are available from the NASA Atmospheric Science Data Center (ASDC; https://asdc.larc.nasa.gov). The ERA5 reanalysis datasets are available from the European Centre for Medium-Range Weather Forecasts (ECMWF) through the Copernicus Climate Data Store at https://cds.climate.copernicus.eu. The analysis code used in this study is available from the corresponding author upon reasonable request.

Author contributions

Y.C. supervised the project. B.Y. developed the analysis code, performed the data analysis, prepared the figures, and wrote the manuscript. J.M. compiled the MODIS and ERA5 datasets. B.Y. and Y.C. interpreted the results with inputs from all co-authors. J.A.K. and N.U. provided critical comments and contributed to the interpretation of the results and manuscript revision.

Competing interests

The authors declare that they have no conflict of interest.

Acknowledgements

This work was supported by the UK Research and Innovation (UKRI) Natural Environment Research Council (NERC) through the project QUESTION (grant number NE/B001024/1). We gratefully acknowledge NASA for providing the MODIS, OMI, and CALIPSO datasets, and the European Centre for Medium-Range Weather Forecasts (ECMWF) for providing the ERA5 reanalysis data used in this study. We also thank the University of Birmingham's BlueBEAR high-performance computing service for providing the computational resources and support that made this work possible.

Financial support

This work was supported by the UK Research and Innovation (UKRI) Natural Environment Research Council (NERC) through the project QUESTION (NE/B001024/1).

References

Ahn, S. H., Yoon, Y. J., Choi, T. J., Lee, J. Y., Kim, Y. P., Lee, B. Y., Ritter, C., Aas, W., Krejci, R., Ström, J., Tunved, P., and Jung, C. H.: Relationship between cloud condensation nuclei (CCN) concentration and aerosol optical depth in the Arctic region, Atmospheric Environment, 267, 118748, https://doi.org/10.1016/j.atmosenv.2021.118748, 2021.

https://doi.org/10.5194/egusphere-2026-3634
Preprint. Discussion started: 8 July 2026

Andreae, M. O.: Correlation between cloud condensation nuclei concentration and aerosol optical thickness in remote and polluted regions, Atmospheric Chemistry and Physics, 9, 543–556, https://doi.org/10.5194/acp-9-543-2009, 2009.

Ångström, A.: On the Atmospheric Transmission of Sun Radiation and on Dust in the Air, Geografiska Annaler, 11, 156–166, https://doi.org/10.2307/519399, 1929.

Belgiu, M. and Drăguţ, L.: Random forest in remote sensing: A review of applications and future directions, ISPRS Journal of Photogrammetry and Remote Sensing, 114, 24–31, https://doi.org/10.1016/j.isprsjprs.2016.01.011, 2016.

Bi, J., Knowland, K. E., Keller, C. A., and Liu, Y.: Combining Machine Learning and Numerical Simulation for High-Resolution PM2.5 Concentration Forecast, Environ. Sci. Technol., 56, 1544–1556, https://doi.org/10.1021/acs.est.1c05578, 2022.

Block, K., Haghighatnasab, M., Partridge, D. G., Stier, P., and Quaas, J.: Cloud condensation nuclei concentrations derived from the CAMS reanalysis, Earth System Science Data, 16, 443–470, https://doi.org/10.5194/essd-16-443-2024, 2024.

Breiman, L.: Random Forests, Machine Learning, 45, 5–32, https://doi.org/10.1023/A:1010933404324, 2001.

Brokamp, C., Jandarov, R., Hossain, M., and Ryan, P.: Predicting Daily Urban Fine Particulate Matter Concentrations Using a Random Forest Model, Environ. Sci. Technol., 52, 4173–4179, https://doi.org/10.1021/acs.est.7b05381, 2018.

Calvin, K., Dasgupta, D., Krinner, G., Mukherji, A., Thorne, P. W., Trisos, C., Romero, J., Aldunce, P., Barrett, K., Blanco, G., Cheung, W. W. L., Connors, S., Denton, F., Diongue-Niang, A., Dodman, D., Garschagen, M., Geden, O., Hayward, B., Jones, C., Jotzo, F., Krug, T., Lasco, R., Lee, Y.-Y., Masson-Delmotte, V., Meinshausen, M., Mintenbeck, K., Mokssit, A., Otto, F. E. L., Pathak, M., Pirani, A., Poloczanska, E., Pörtner, H.-O., Revi, A., Roberts, D. C., Roy, J., Ruane, A. C., Skea, J., Shukla, P. R., Slade, R., Slangen, A., Sokona, Y., Sörensson, A. A., Tignor, M., Van Vuuren, D., Wei, Y.-M., Winkler, H., Zhai, P., Zommers, Z., Hourcade, J.-C., Johnson, F. X., Pachauri, S., Simpson, N. P., Singh, C., Thomas, A., Totin, E., Alegría, A., Armour, K., Bednar-Friedl, B., Blok, K., Cissé, G., Dentener, F., Eriksen, S., Fischer, E., Garner, G., Guivarch, C., Haasnoot, M., Hansen, G., Hauser, M., Hawkins, E., Hermans, T., Kopp, R., Leprince-Ringuet, N., Lewis, J., Ley, D., Ludden, C., Niamir, L., Nicholls, Z., Some, S., Szopa, S., Trewin, B., Van Der Wijst, K.-I., Winter, G., Witting, M., Birt, A., and Ha, M.: IPCC, 2023: Climate Change 2023: Synthesis Report. Contribution of Working Groups I, II and III to the Sixth Assessment Report of the Intergovernmental Panel on Climate Change [Core Writing Team, H. Lee and J. Romero (eds.)]. IPCC, Geneva, Switzerland., Intergovernmental Panel on Climate Change (IPCC), https://doi.org/10.59327/IPCC/AR6-9789291691647, 2023.

Chen, G. and Wang, W.-C.: Aerosol–Stratocumulus–Radiation Interactions over the Southeast Pacific: Implications to the Underlying Air–Sea Coupling, Journal of the Atmospheric Sciences, 73, 2759–2771, https://doi.org/10.1175/JAS-D-15-0277.1, 2016.

Chen, G., Wang, W.-C., and Chen, J.-P.: Aerosol–Stratocumulus–Radiation Interactions over the Southeast Pacific, Journal of the Atmospheric Sciences, 72, 2612–2621, https://doi.org/10.1175/JAS-D-14-0319.1, 2015.

Chen, Y., Cheng, Y.-F., Nordmann, S., Birmili, W., Denier van der Gon, H. A. C., Ma, N., Wolke, R., Wehner, B., Sun, J., Spindler, G., Mu, Q., Pöschl, U., Su, H., and Wiedensohler, A.: Evaluation of the size segregation of elemental carbon (EC) emission in Europe: influence on the simulation of EC long-range transportation, Atmospheric Chemistry and Physics, 16, 1823–1835, https://doi.org/10.5194/acp-16-1823-2016, 2016.

Chen, Y., Haywood, J., Wang, Y., Malavelle, F., Jordan, G., Partridge, D., Fieldsend, J., De Leeuw, J., Schmidt, A., Cho, N., Oreopoulos, L., Platnick, S., Grosvenor, D., Field, P., and Lohmann, U.: Machine learning reveals climate forcing from aerosols is dominated by increased cloud cover, Nat. Geosci., 15, 609–614, https://doi.org/10.1038/s41561-022-00991-6, 2022.

Chen, Y., Haywood, J., Wang, Y., Malavelle, F., Jordan, G., Peace, A., Partridge, D. G., Cho, N., Oreopoulos, L., Grosvenor, D., Field, P., Allan, R. P., and Lohmann, U.: Substantial cooling effect from aerosol-induced increase in tropical marine cloud cover, Nat. Geosci., 17, 404–410, https://doi.org/10.1038/s41561-024-01427-z, 2024.

Choudhury, G. and Tesche, M.: Global multiyear 3D dataset of cloud condensation nuclei derived from spaceborne lidar measurements, https://doi.org/10.1594/PANGAEA.956215, 2023.

Christensen, M. W., Gettelman, A., Cermak, J., Dagan, G., Diamond, M., Douglas, A., Feingold, G., Glassmeier, F., Goren, T., Grosvenor, D. P., Gryspeerdt, E., Kahn, R., Li, Z., Ma, P.-L., Malavelle, F., McCoy, I. L., McCoy, D. T., McFarquhar, G., Mülmenstädt, J., Pal, S., Possner, A., Povey, A., Quaas, J., Rosenfeld, D., Schmidt, A., Schrödner,

https://doi.org/10.5194/egusphere-2026-3634
Preprint. Discussion started: 8 July 2026

R., Sorooshian, A., Stier, P., Toll, V., Watson-Parris, D., Wood, R., Yang, M., and Yuan, T.: Opportunistic experiments to constrain aerosol effective radiative forcing, Atmospheric Chemistry and Physics, 22, 641–674, https://doi.org/10.5194/acp-22-641-2022, 2022.

Damany-Pearce, L., Johnson, B., Wells, A., Osborne, M., Allan, J., Belcher, C., Jones, A., and Haywood, J.: Australian wildfires cause the largest stratospheric warming since Pinatubo and extends the lifetime of the Antarctic ozone hole, Sci Rep, 12, 12665, https://doi.org/10.1038/s41598-022-15794-3, 2022.

Deng, Z. Z., Zhao, C. S., Ma, N., Liu, P. F., Ran, L., Xu, W. Y., Chen, J., Liang, Z., Liang, S., Huang, M. Y., Ma, X. C., Zhang, Q., Quan, J. N., Yan, P., Henning, S., Mildenberger, K., Sommerhage, E., Schäfer, M., Stratmann, F., and Wiedensohler, A.: Size-resolved and bulk activation properties of aerosols in the North China Plain, Atmospheric Chemistry and Physics, 11, 3835–3846, https://doi.org/10.5194/acp-11-3835-2011, 2011.

Ding, S., Zhao, D., He, C., Huang, M., He, H., Tian, P., Liu, Q., Bi, K., Yu, C., Pitt, J., Chen, Y., Ma, X., Chen, Y., Jia, X., Kong, S., Wu, J., Hu, D., Hu, K., Ding, D., and Liu, D.: Observed Interactions Between Black Carbon and Hydrometeor During Wet Scavenging in Mixed-Phase Clouds, Geophysical Research Letters, 46, 8453–8463, https://doi.org/10.1029/2019GL083171, 2019.

Dusek, U., Frank, G. P., Hildebrandt, L., Curtius, J., Schneider, J., Walter, S., Chand, D., Drewnick, F., Hings, S., Jung, D., Borrmann, S., and Andreae, M. O.: Size Matters More Than Chemistry for Cloud-Nucleating Ability of Aerosol Particles, Science, 312, 1375–1378, https://doi.org/10.1126/science.1125261, 2006a.

Dusek, U., Frank, G. P., Hildebrandt, L., Curtius, J., Schneider, J., Walter, S., Chand, D., Drewnick, F., Hings, S., Jung, D., Borrmann, S., and Andreae, M. O.: Size Matters More Than Chemistry for Cloud-Nucleating Ability of Aerosol Particles, Science, 312, 1375–1378, https://doi.org/10.1126/science.1125261, 2006b.

Edwards, E.-L., Corral, A. F., Dadashazar, H., Barkley, A. E., Gaston, C. J., Zuidema, P., and Sorooshian, A.: Impact of various air mass types on cloud condensation nuclei concentrations along coastal southeast Florida, Atmospheric Environment, 254, 118371, https://doi.org/10.1016/j.atmosenv.2021.118371, 2021.

Forster, P., Storelvmo, T., Armour, K., and Collins, W.: The Earth's Energy Budget, Climate Feedbacks, and Climate Sensitivity, in: Climate Change 2021: The Physical Science Basis, Cambridge University Press, 923–1054, https://doi.org/10.1017/9781009157896.009, 2023.

Gryspeerdt, E., Povey, A. C., Grainger, R. G., Hasekamp, O., Hsu, N. C., Mulcahy, J. P., Sayer, A. M., and Sorooshian, A.: Uncertainty in aerosol–cloud radiative forcing is driven by clean conditions, Atmospheric Chemistry and Physics, 23, 4115–4122, https://doi.org/10.5194/acp-23-4115-2023, 2023.

Hasekamp, O. P., Gryspeerdt, E., and Quaas, J.: Analysis of polarimetric satellite measurements suggests stronger cooling due to aerosol-cloud interactions, Nat Commun, 10, 5405, https://doi.org/10.1038/s41467-019-13372-2, 2019.

Herbert, R. and Stier, P.: Satellite observations of smoke–cloud–radiation interactions over the Amazon rainforest, Atmospheric Chemistry and Physics, 23, 4595–4616, https://doi.org/10.5194/acp-23-4595-2023, 2023.

Hersbach, H., Bell, B., Berrisford, P., Hirahara, S., Horányi, A., Muñoz-Sabater, J., Nicolas, J., Peubey, C., Radu, R., Schepers, D., Simmons, A., Soci, C., Abdalla, S., Abellan, X., Balsamo, G., Bechtold, P., Biavati, G., Bidlot, J., Bonavita, M., De Chiara, G., Dahlgren, P., Dee, D., Diamantakis, M., Dragani, R., Flemming, J., Forbes, R., Fuentes, M., Geer, A., Haimberger, L., Healy, S., Hogan, R. J., Hólm, E., Janisková, M., Keeley, S., Laloyaux, P., Lopez, P., Lupu, C., Radnoti, G., de Rosnay, P., Rozum, I., Vamborg, F., Villaume, S., and Thépaut, J.-N.: The ERA5 global reanalysis, Quarterly Journal of the Royal Meteorological Society, 146, 1999–2049, https://doi.org/10.1002/qj.3803, 2020.

Hodshire, A. L., Bian, Q., Ramnarine, E., Lonsdale, C. R., Alvarado, M. J., Kreidenweis, S. M., Jathar, S. H., and Pierce, J. R.: More Than Emissions and Chemistry: Fire Size, Dilution, and Background Aerosol Also Greatly Influence Near-Field Biomass Burning Aerosol Aging, Journal of Geophysical Research: Atmospheres, 124, 5589–5611, https://doi.org/10.1029/2018JD029674, 2019.

Huang, X., Ding, K., Liu, J., Wang, Z., Tang, R., Xue, L., Wang, H., Zhang, Q., Tan, Z.-M., Fu, C., Davis, S. J., Andreae, M. O., and Ding, A.: Smoke-weather interaction affects extreme wildfires in diverse coastal regions, Science, 379, 457–461, https://doi.org/10.1126/science.add9843, 2023.

Jethva, H., Torres, O., and Ahn, C.: A 12-year long global record of optical depth of absorbing aerosols above the clouds derived from the OMI/OMACA algorithm, Atmospheric Measurement Techniques, 11, 5837–5864, https://doi.org/10.5194/amt-11-5837-2018, 2018.

https://doi.org/10.5194/egusphere-2026-3634
Preprint. Discussion started: 8 July 2026

Jia, H., Ma, X., Yu, F., and Quaas, J.: Significant underestimation of radiative forcing by aerosol–cloud interactions derived from satellite-based methods, Nat Commun, 12, 3649, https://doi.org/10.1038/s41467-021-23888-1, 2021.

Jin, J., Henzing, B., and Segers, A.: How aerosol size matters in aerosol optical depth (AOD) assimilation and the optimization using the Ångström exponent, Atmospheric Chemistry and Physics, 23, 1641–1660, https://doi.org/10.5194/acp-23-1641-2023, 2023.

June, N. A., Hodshire, A. L., Wiggins, E. B., Winstead, E. L., Robinson, C. E., Thornhill, K. L., Sanchez, K. J., Moore, R. H., Pagonis, D., Guo, H., Campuzano-Jost, P., Jimenez, J. L., Coggon, M. M., Dean-Day, J. M., Bui, T. P., Peischl, J., Yokelson, R. J., Alvarado, M. J., Kreidenweis, S. M., Jathar, S. H., and Pierce, J. R.: Aerosol size distribution changes in FIREX-AQ biomass burning plumes: the impact of plume concentration on coagulation and OA condensation/evaporation, Atmospheric Chemistry and Physics, 22, 12803–12825, https://doi.org/10.5194/acp-22-12803-2022, 2022.

Kaufman, Y. J. and Koren, I.: Smoke and Pollution Aerosol Effect on Cloud Cover, Science, 313, 655–658, https://doi.org/10.1126/science.1126232, 2006.

Köhler, H.: The nucleus in and the growth of hygroscopic droplets, Trans. Faraday Soc., 32, 1152–1161, https://doi.org/10.1039/TF9363201152, 1936.

Li, T., Guo, Y., Liu, Y., Wang, J., Wang, Q., Sun, Z., He, M. Z., and Shi, X.: Estimating mortality burden attributable to short-term PM2.5 exposure: A national observational study in China, Environment International, 125, 245–251, https://doi.org/10.1016/j.envint.2019.01.073, 2019.

Li, Y., Santer, B. D., Solomon, S., Thompson, D. W. J., and Fu, Q.: Detectable global temperature responses to wildfires and volcanic eruptions, Proceedings of the National Academy of Sciences, 123, e2525500123, https://doi.org/10.1073/pnas.2525500123, 2026.

Liu, J. and Li, Z.: Estimation of cloud condensation nuclei concentration from aerosol optical quantities: influential factors and uncertainties, Atmospheric Chemistry and Physics, 14, 471–483, https://doi.org/10.5194/acp-14-471-2014, 2014.

Liu, L., Cheng, Y., Wang, S., Wei, C., Pöhlker, M. L., Pöhlker, C., Artaxo, P., Shrivastava, M., Andreae, M. O., Pöschl, U., and Su, H.: Impact of biomass burning aerosols on radiation, clouds, and precipitation over the Amazon: relative importance of aerosol–cloud and aerosol–radiation interactions, Atmospheric Chemistry and Physics, 20, 13283–13301, https://doi.org/10.5194/acp-20-13283-2020, 2020.

Lv, L., Wei, P., Li, J., and Hu, J.: Application of machine learning algorithms to improve numerical simulation prediction of PM2.5 and chemical components, Atmospheric Pollution Research, 12, 101211, https://doi.org/10.1016/j.apr.2021.101211, 2021.

Ma, C., Su, H., Lelieveld, J., Randel, W., Yu, P., Andreae, M. O., and Cheng, Y.: Smoke-charged vortex doubles hemispheric aerosol in the middle stratosphere and buffers ozone depletion, Science Advances, 10, eadn3657, https://doi.org/10.1126/sciadv.adn3657, 2024.

Ma, P.-L., Rasch, P. J., Chepfer, H., Winker, D. M., and Ghan, S. J.: Observational constraint on cloud susceptibility weakened by aerosol retrieval limitations, Nat Commun, 9, 2640, https://doi.org/10.1038/s41467-018-05028-4, 2018.

Myers, T. A., Scott, R. C., Zelinka, M. D., Klein, S. A., Norris, J. R., and Caldwell, P. M.: Observational constraints on low cloud feedback reduce uncertainty of climate sensitivity, Nat. Clim. Chang., 11, 501–507, https://doi.org/10.1038/s41558-021-01039-0, 2021.

Ohneiser, K., Ansmann, A., Baars, H., Seifert, P., Barja, B., Jimenez, C., Radenz, M., Teisseire, A., Floutsi, A., Haarig, M., Foth, A., Chudnovsky, A., Engelmann, R., Zamorano, F., Bühl, J., and Wandinger, U.: Smoke of extreme Australian bushfires observed in the stratosphere over Punta Arenas, Chile, in January 2020: optical thickness, lidar ratios, and depolarization ratios at 355 and 532 nm, Atmospheric Chemistry and Physics, 20, 8003–8015, https://doi.org/10.5194/acp-20-8003-2020, 2020.

Painemal, D., Chang, F.-L., Ferrare, R., Burton, S., Li, Z., Smith Jr., W. L., Minnis, P., Feng, Y., and Clayton, M.: Reducing uncertainties in satellite estimates of aerosol–cloud interactions over the subtropical ocean by integrating vertically resolved aerosol observations, Atmospheric Chemistry and Physics, 20, 7167–7177, https://doi.org/10.5194/acp-20-7167-2020, 2020.

https://doi.org/10.5194/egusphere-2026-3634
Preprint. Discussion started: 8 July 2026

Pawan K. Bhartia: OMI/Aura TOMS-Like Ozone, Aerosol Index, Cloud Radiance Fraction L3 1 day 1 degree x 1 degree V3, NASA Goddard Space Flight Center, 2012.

Peterson, D. A., Fromm, M. D., McRae, R. H. D., Campbell, J. R., Hyer, E. J., Taha, G., Camacho, C. P., Kablick, G. P., Schmidt, C. C., and DeLand, M. T.: Australia's Black Summer pyrocumulonimbus super outbreak reveals potential for increasingly extreme stratospheric smoke events, npj Clim Atmos Sci, 4, 38, https://doi.org/10.1038/s41612-021-00192-9, 2021.

Petters, M. D. and Kreidenweis, S. M.: A single parameter representation of hygroscopic growth and cloud condensation nucleus activity, Atmospheric Chemistry and Physics, 7, 1961–1971, https://doi.org/10.5194/acp-7-1961-2007, 2007.

Pierce, J. R., Chen, K., and Adams, P. J.: Contribution of primary carbonaceous aerosol to cloud condensation nuclei: processes and uncertainties evaluated with a global aerosol microphysics model, Atmospheric Chemistry and Physics, 7, 5447–5466, https://doi.org/10.5194/acp-7-5447-2007, 2007.

Quaas, J., Arola, A., Cairns, B., Christensen, M., Deneke, H., Ekman, A. M. L., Feingold, G., Fridlind, A., Gryspeerdt, E., Hasekamp, O., Li, Z., Lipponen, A., Ma, P.-L., Mülmenstädt, J., Nenes, A., Penner, J. E., Rosenfeld, D., Schrödner, R., Sinclair, K., Sourdeval, O., Stier, P., Tesche, M., van Diedenhoven, B., and Wendisch, M.: Constraining the Twomey effect from satellite observations: issues and perspectives, Atmospheric Chemistry and Physics, 20, 15079–15099, https://doi.org/10.5194/acp-20-15079-2020, 2020.

Ramnarine, E., Kodros, J. K., Hodshire, A. L., Lonsdale, C. R., Alvarado, M. J., and Pierce, J. R.: Effects of near-source coagulation of biomass burning aerosols on global predictions of aerosol size distributions and implications for aerosol radiative effects, Atmospheric Chemistry and Physics, 19, 6561–6577, https://doi.org/10.5194/acp-19-6561-2019, 2019.

Reid, J. S., Koppmann, R., Eck, T. F., and Eleuterio, D. P.: A review of biomass burning emissions part II: intensive physical properties of biomass burning particles, Atmospheric Chemistry and Physics, 5, 799–825, https://doi.org/10.5194/acp-5-799-2005, 2005.

Roberts, G. C., Nenes, A., Seinfeld, J. H., and Andreae, M. O.: Impact of biomass burning on cloud properties in the Amazon Basin, Journal of Geophysical Research: Atmospheres, 108, https://doi.org/10.1029/2001JD000985, 2003.

Romakkaniemi, S., Arola, A., Kokkola, H., Birmili, W., Tuch, T., Kerminen, V.-M., Räisänen, P., Smith, J. N., Korhonen, H., and Laaksonen, A.: Effect of aerosol size distribution changes on AOD, CCN and cloud droplet concentration: Case studies from Erfurt and Melpitz, Germany, Journal of Geophysical Research: Atmospheres, 117, https://doi.org/10.1029/2011JD017091, 2012.

Rosenfeld, D., Lohmann, U., Raga, G. B., O'Dowd, C. D., Kulmala, M., Fuzzi, S., Reissell, A., and Andreae, M. O.: Flood or Drought: How Do Aerosols Affect Precipitation?, Science, 321, 1309–1313, https://doi.org/10.1126/science.1160606, 2008.

Rosenfeld, D., Kokhanovsky, A., Goren, T., Gryspeerdt, E., Hasekamp, O., Jia, H., Lopatin, A., Quaas, J., Pan, Z., and Sourdeval, O.: Frontiers in Satellite-Based Estimates of Cloud-Mediated Aerosol Forcing, Reviews of Geophysics, 61, e2022RG000799, https://doi.org/10.1029/2022RG000799, 2023.

Sakamoto, K. M., Laing, J. R., Stevens, R. G., Jaffe, D. A., and Pierce, J. R.: The evolution of biomass-burning aerosol size distributions due to coagulation: dependence on fire and meteorological details and parameterization, Atmospheric Chemistry and Physics, 16, 7709–7724, https://doi.org/10.5194/acp-16-7709-2016, 2016.

Scornet, E., Biau, G., and Vert, J.-P.: Consistency of random forests, The Annals of Statistics, 43, 1716–1741, https://doi.org/10.1214/15-AOS1321, 2015.

Scott, R. C., Myers, T. A., Norris, J. R., Zelinka, M. D., Klein, S. A., Sun, M., and Doelling, D. R.: Observed Sensitivity of Low-Cloud Radiative Effects to Meteorological Perturbations over the Global Oceans, Journal of Climate, 33, 7717–7734, https://doi.org/10.1175/JCLI-D-19-1028.1, 2020.

Sokolik, I. N., Soja, A. J., DeMott, P. J., and Winker, D.: Progress and Challenges in Quantifying Wildfire Smoke Emissions, Their Properties, Transport, and Atmospheric Impacts, Journal of Geophysical Research: Atmospheres, 124, 13005–13025, https://doi.org/10.1029/2018JD029878, 2019.

Spracklen, D. V., Carslaw, K. S., Pöschl, U., Rap, A., and Forster, P. M.: Global cloud condensation nuclei influenced by carbonaceous combustion aerosol, Atmospheric Chemistry and Physics, 11, 9067–9087, https://doi.org/10.5194/acp-11-9067-2011, 2011.

https://doi.org/10.5194/egusphere-2026-3634
Preprint. Discussion started: 8 July 2026

Stier, P.: Limitations of passive remote sensing to constrain global cloud condensation nuclei, Atmospheric Chemistry and Physics, 16, 6595–6607, https://doi.org/10.5194/acp-16-6595-2016, 2016.

Textor, C., Schulz, M., Guibert, S., Kinne, S., Balkanski, Y., Bauer, S., Berntsen, T., Berglen, T., Boucher, O., Chin, M., Dentener, F., Diehl, T., Easter, R., Feichter, H., Fillmore, D., Ghan, S., Ginoux, P., Gong, S., Grini, A., Hendricks, J., Horowitz, L., Huang, P., Isaksen, I., Iversen, I., Kloster, S., Koch, D., Kirkevåg, A., Kristjansson, J. E., Krol, M., Lauer, A., Lamarque, J. F., Liu, X., Montanaro, V., Myhre, G., Penner, J., Pitari, G., Reddy, S., Seland, Ø., Stier, P., Takemura, T., and Tie, X.: Analysis and quantification of the diversities of aerosol life cycles within AeroCom, Atmospheric Chemistry and Physics, 6, 1777–1813, https://doi.org/10.5194/acp-6-1777-2006, 2006.

Tian, P., Liu, D., Zhao, D., Yu, C., Liu, Q., Huang, M., Deng, Z., Ran, L., Wu, Y., Ding, S., Hu, K., Zhao, G., Zhao, C., and Ding, D.: In situ vertical characteristics of optical properties and heating rates of aerosol over Beijing, Atmospheric Chemistry and Physics, 20, 2603–2622, https://doi.org/10.5194/acp-20-2603-2020, 2020.

Torres, O., Bhartia, P. K., Herman, J. R., Ahmad, Z., and Gleason, J.: Derivation of aerosol properties from satellite measurements of backscattered ultraviolet radiation: Theoretical basis, Journal of Geophysical Research: Atmospheres, 103, 17099–17110, https://doi.org/10.1029/98JD00900, 1998.

Twomey, S.: Pollution and the planetary albedo, Atmospheric Environment (1967), 8, 1251–1256, https://doi.org/10.1016/0004-6981(74)90004-3, 1974.

Twomey, S.: The Influence of Pollution on the Shortwave Albedo of Clouds, 1977.

Vakkari, V., Kerminen, V.-M., Beukes, J. P., Tiitta, P., van Zyl, P. G., Josipovic, M., Venter, A. D., Jaars, K., Worsnop, D. R., Kulmala, M., and Laakso, L.: Rapid changes in biomass burning aerosols by atmospheric oxidation, Geophysical Research Letters, 41, 2644–2651, https://doi.org/10.1002/2014GL059396, 2014.

van der Velde, I. R., van der Werf, G. R., Houweling, S., Maasakkers, J. D., Borsdorff, T., Landgraf, J., Tol, P., van Kempen, T. A., van Hees, R., Hoogeveen, R., Veefkind, J. P., and Aben, I.: Vast CO2 release from Australian fires in 2019–2020 constrained by satellite, Nature, 597, 366–369, https://doi.org/10.1038/s41586-021-03712-y, 2021.

Xiao, Q., Chang, H. H., Geng, G., and Liu, Y.: An Ensemble Machine-Learning Model To Predict Historical PM2.5 Concentrations in China from Satellite Data, Environ. Sci. Technol., 52, 13260–13269, https://doi.org/10.1021/acs.est.8b02917, 2018.

Yang, X., Zhao, C., Yang, Y., Yan, X., and Fan, H.: Statistical aerosol properties associated with fire events from 2002 to 2019 and a case analysis in 2019 over Australia, Atmospheric Chemistry and Physics, 21, 3833–3853, https://doi.org/10.5194/acp-21-3833-2021, 2021.

Yu, P., Davis, S. M., Toon, O. B., Portmann, R. W., Bardeen, C. G., Barnes, J. E., Telg, H., Maloney, C., and Rosenlof, K. H.: Persistent Stratospheric Warming Due to 2019–2020 Australian Wildfire Smoke, Geophysical Research Letters, 48, e2021GL092609, https://doi.org/10.1029/2021GL092609, 2021.

Zheng, G., Sedlacek, A. J., Aiken, A. C., Feng, Y., Watson, T. B., Raveh-Rubin, S., Uin, J., Lewis, E. R., and Wang, J.: Long-range transported North American wildfire aerosols observed in marine boundary layer of eastern North Atlantic, Environment International, 139, 105680, https://doi.org/10.1016/j.envint.2020.105680, 2020.